4-10-2016

Double Power Laws In The Event-Integrated Solar Energetic Particle Spectrum

Lulu Zhao

Ming Zhang

Hamid K. Rassoul

The Astrophysical Journal, 821:62 (9pp), 2016 April 10 doi:10.3847/0004-637X/821/1/62

DOUBLE POWER LAWS IN THE EVENT-INTEGRATED SOLAR ENERGETIC PARTICLE SPECTRUM

Lulu Zhao, Ming Zhang, and Hamid K. Rassoul
Physics and Space Sciences Department, Florida Institute of Technology, Melbourne, FL 32901, USA; lzhao@fit.edu
Received 2016 January 12; accepted 2016 February 20; published 2016 April 11

ABSTRACT

A double power law or a power law with exponential rollover at a few to tens of MeV nucleon^{-1} of the event-integrated differential spectra has been reported in many solar energetic particle (SEP) events. The rollover energies per nucleon of different elements correlate with a particle's charge-to-mass ratio (Q/A). The probable causes are suggested as residing in shock finite lifetimes, shock finite sizes, shock geometry, and an adiabatic cooling effect. In this work, we conduct a numerical simulation to investigate a particle's transport process in the inner heliosphere. We solve the focused transport equation using a time-backward Markov stochastic approach. The convection, magnetic focusing, adiabatic cooling effect, and pitch-angle scattering are included. The effects that the interplanetary turbulence imposes on the shape of the resulting SEP spectra are examined. By assuming a pure power-law differential spectrum at the Sun, a perfect double-power-law feature with a break energy ranging from 10 to 120 MeV nucleon^{-1} is obtained at 1 au. We found that the double power law of the differential energy spectrum is a robust result of SEP interplanetary propagation. It works for many assumptions of interplanetary turbulence spectra that give various forms of momentum dependence of a particle's mean free path. The different spectral shapes in low-energy and high-energy ends are not just a transition from the convection-dominated propagation to diffusion-dominated propagation.

Key words: interplanetary medium – Sun: particle emission

1. INTRODUCTION

There are two physical mechanisms for accelerating energetic particles in solar energetic particle (SEP) events, corresponding to impulsive and gradual events (see Reames 2013, and references therein). Impulsive events are often associated with solar flares, in which energetic particles can be accelerated by resonating with cascading magnetohydrodynamic waves in the magnetic reconnection process (Miller 1998). Gradual events are often accompanied by coronal mass ejections (CMEs). In the vicinity of the shock driven by a CME, particles can be accelerated through the first-order Fermi acceleration (e.g., Axford et al. 1977; Krymsky 1977), yielding a power-law energy spectrum (Blandford & Ostriker 1978). The power-law index is fully determined by shock properties and is independent of species (Lee 1983).

However, in many large SEP events, rather than exhibiting a single power law, the event-integrated spectra indices were distinct in different species (e.g., Tylka et al. 2002; Cohen et al. 2003). For instance, iron spectra were either harder or softer than oxygen above tens of MeV nucleon^{-1} (Tylka et al. 1997, 2005). In addition, the energy spectra often show breaks at a few to tens of MeV nucleon^{-1} (Mazur et al. 1992; Tylka et al. 2000, 2005; Cohen et al. 2005; Mewaldt et al. 2005a). The event-integrated spectra can be described either by a power law with exponential rollover (Ellison–Ramaty form; Ellison & Ramaty 1985),

$$\frac{dJ}{dE} = E^{-\gamma}\exp\left(-\frac{E}{E_0}\right), \tag{1}$$

where E is the particle's kinetic energy per nucleon, E_0 is the break energy per nucleon, and γ is the energy spectrum index, or by a double power law (Band et al. 1993),

$$\frac{dJ}{dE} = \begin{cases} E^{-\alpha}\exp\left(-\frac{E}{E_0}\right) & E \leqslant (\beta-\alpha)E_0, \\ E^{-\beta}[(\beta-\alpha)E_0]^{\beta-\alpha}\exp(\alpha-\beta) & E \geqslant (\beta-\alpha)E_0. \end{cases} \tag{2}$$

Here α is the power-law index for low-energy particles and β is the power-law index for high-energy particles.

Mewaldt et al. (2005a, 2005b) surveyed the H, He, and O spectra in large SEP events during 2003 October–November and 2005 January and found that the Ellison–Ramaty form (Ellison & Ramaty 1985) only fits the lower part of the energy spectra. Instead, the energy spectra are better fit by double power laws. Later, Mewaldt et al. (2012) analyzed the proton energy spectra in 16 ground-level enhancement events in solar cycle 23 and found that the spectra are well fit by a double power law up to 700 MeV. Recent studies found that the e-folding energy E_0 also evolves with time (Tylka et al. 2000), and the break energy is ordered by a particle's charge-to-mass (Q/A) ratio for different ion species (Cohen et al. 2005; Tylka et al. 2005). The cause of the ordering of the break energy with Q/A was examined by Cohen et al. (2005), Zank et al. (2000), and Li & Zank (2005). It was suggested that it resides in the different mean free paths of different species in the shock region. The "step-like" behavior of the diffusion coefficient as a function of the rigidity allows energetic particles to escape (thus reaching the maximum achievable energy) from the shock region at the same rigidity. Thus, the resulting energy spectra break at the same rigidity (i.e., different energy per nucleon).

The effect of the evolutionary history of shock geometry on the spectral shape in SEP events was first discussed by Tylka et al. (2005) and Tylka & Lee (2006). Later the quantity

connection between the shock geometry and the spectral break energy was studied theoretically and numerically by Li et al. (2009). They concluded that the break energy in a quasi-parallel shock has a stronger Q/A dependence ($E_0 \sim (Q/A)^{\delta}$ with $\delta \sim 2$) than a quasi-perpendicular shock ($\delta \sim 1/5$). Mason et al. (2012) investigated the interplanetary propagation of SEPs using a transport model, including convection, adiabatic cooling, pitch-angle scattering, and the magnetic focusing effect. They suggested that the transport process does not modify the spectrum much. Instead, the spectrum breaks must have existed at the source. Recently, Li & Lee (2015) analytically solved the SEP differential fluence from the Parker diffusion equation with a few assumptions to simplify the Parker equation. They found that the interplanetary transport can change the spectrum of SEP fluence seen at 1 astronomical unit (au), producing up to three distinctive power laws at 1 au. By fitting the analytical results with observations, they suggested that the scatter-dominated interplanetary transport plays an important role in bending the initial power-law source spectrum around 10 MeV in well-connected events. The spectral breaks in the near-central meridian events are still dominated by the interplanetary shock acceleration. In this work, we numerically solved the focused transport equation using a Monte Carlo simulation. Adiabatic cooling in the expanding solar wind, pitch-angle diffusion in the turbulent interplanetary magnetic field, magnetic focusing, and convection effects are included. Our simulation showed that a double power law is obtained at 1 au from a single power-law source spectrum at the Sun. This is consistent with the conclusion made by Li & Lee (2015), but our numerical solutions showed that the result is far more robust than the condition assumed by Li & Lee (2015).

This paper is organized as follows. In Section 2 we discuss the numerical model. Section 3 describes the interplanetary turbulence spectrum. We present our results in Section 4. Section 5 contains a discussion based on the numerical results, and Section 6 summarizes the conclusion.

2. METHODS

The transport of energetic particles in the inner heliosphere can be described by the focused transport equation (Skilling 1971; Qin et al. 2004, 2006; Zhang 2006; Zhang et al. 2009)

$$\frac{\partial f}{\partial t} + \mu v \frac{\partial f}{\partial z} + \boldsymbol{V}^{\rm sw} \cdot \nabla f + \frac{dp}{dt}\frac{\partial f}{\partial p} + \frac{d\mu}{dt}\frac{\partial f}{\partial \mu} - \frac{\partial}{\partial \mu}\left(D_{\mu\mu}\frac{\partial f}{\partial \mu}\right) = Q, \quad (3)$$

where f is the particle's distribution function, μ is the particle's pitch-angle cosine, $\boldsymbol{V}^{\rm sw}$ is the solar wind velocity, p is the particle's momentum in the solar wind frame, z is the direction along the interplanetary magnetic field (Parker spiral), and the right-hand side is the source term. The dp/dt term describes the adiabatic cooling effect, and the $d\mu/dt$ term describes the magnetic focusing effect and the effect due to solar wind expansion. Those two terms can be written as (Roelof 1969, p. 111; Skilling 1971; Isenberg 1997; Kóta & Jokipii 1997; Qin et al. 2004, 2006)

$$\frac{dp}{dt} = -p\left[\frac{1-\mu^2}{2}\left(\frac{\partial V_x^{\rm sw}}{\partial x} + \frac{\partial V_y^{\rm sw}}{\partial y}\right) + \mu^2 \frac{\partial V_z^{\rm sw}}{\partial z}\right], \quad (4)$$

$$\frac{d\mu}{dt} = \frac{1-\mu^2}{2}\left[\frac{v}{L} + \mu\left(\frac{\partial V_x^{\rm sw}}{\partial x} + \frac{\partial V_y^{\rm sw}}{\partial y} - 2\frac{\partial V_z^{\rm sw}}{\partial z}\right)\right]. \quad (5)$$

Here B is the background magnetic field and L is its scale length, defined as

$$\frac{1}{L} = -\frac{1}{B}\frac{\partial B}{\partial z}. \quad (6)$$

In the focused transport approach, a particle's gyrophase is averaged out and the particle's motion is reduced to the guiding center's motion along the interplanetary magnetic field and diffusion due to magnetic turbulence. In quasi-linear theory (Jokipii 1966), a particle's interaction with magnetic turbulence is approximated by a pitch-angle scattering in the form of $\partial(D_{\mu\mu}\partial f/\partial\mu)/\partial\mu$. $D_{\mu\mu}$, the pitch-angle diffusion coefficient, is given by (Jokipii 1971; Lee & Lerche 1974; Wentzel 1974; Decker 1988)

$$D_{\mu\mu} = \frac{1}{2}\frac{\langle(\Delta\mu)^2\rangle}{\Delta t} = \frac{\pi}{4}(1-\mu^2)\Omega_0 \frac{k_r P(k_r)}{B_0^2}, \quad (7)$$

where $k_r = \Omega_0/(v|\mu|)$ is the resonant wavenumber, $\Omega_0 = qB/m$ is the particle's gyrofrequency with the mass m and the charge q, and $P(k_r)$ is the power spectrum of the turbulence. $P(k_r)$ is proportional to the turbulence level $(\delta B)^2$. The radial dependence of the interplanetary turbulence level $(\delta B)^2$ is currently unknown. Therefore, the radial dependence of $D_{\mu\mu}$ is unknown. In this work, we assume that the particle's radial mean free path λ_r is a constant at all distances. The radial mean free path λ_r relates to the parallel mean free path $\lambda_\parallel$ through

$$\lambda_r = \lambda_\parallel \cos^2\psi, \quad (8)$$

where ψ is the angle between the radial direction and the local magnetic field direction. At 1 au, $\psi \sim 45^\circ$ and $\lambda_r \sim 0.5\lambda_\parallel$. The particle's parallel mean free path to the background magnetic field is related to $D_{\mu\mu}$ by (Jokipii 1966; Earl 1974; Decker 1988)

$$\lambda_\parallel = \frac{3v}{4}\int_0^1 \frac{(1-\mu^2)^2}{D_{\mu\mu}} d\mu. \quad (9)$$

Substituting Equation (7) into Equation (9), we get

$$\lambda_\parallel = \frac{3}{\pi}R^2 \int_0^1 (1-\mu^2)|\mu| \frac{1}{P(k_r)} d\mu, \quad (10)$$

where $R = mv/q$ is the particle's rigidity with the velocity v. Apparently, $\lambda_\parallel$ is determined by the interplanetary turbulence and the particle's rigidity R.

In this calculation, particles are followed using the time-backward Markov stochastic equation (Zhang 1999; Qin et al. 2006). Energetic particles with energies E_i (100 keV nucleon^{-1}, 300 keV nucleon^{-1}, 1 MeV nucleon^{-1}, 3 MeV nucleon^{-1}, 10 MeV nucleon^{-1}, 30 MeV nucleon^{-1}, 100 MeV nucleon^{-1}, 300 MeV nucleon^{-1}, and 1 GeV nucleon^{-1}) and pitch-angle cosine μ_i (-1.0, 0.0 and 1.0) are injected at 1 au and traced back to the Sun through different stochastic processes. The simulation stops when the particles reach the

Table 1
Element Charge States

Element	Mass	Charge
He	4	2
O	16	7
Mg	24	9
Fe	52	12

Note. Charge states can be found in Cohen et al. (2005) and references therein.

inner ($r_{\rm in} = 0.05$ au) or outer ($r_{\rm out} = 50$ au) boundaries or the time exceeds the time limit ($T = 5$ days). The solar wind speed is set to be 400 km s^{-1}, and the magnetic field is set to be a Parker spiral. The magnetic field strength B is assumed to be 5 nT at 1 au. The source is specified as a boundary condition at $r_0 = 0.05$ au with a power-law spectrum γ_0, described by (Reid 1964; Qin et al. 2006)

$$f_b(r_0) = \frac{C}{t}\frac{E_k^{-\gamma_0}}{p_k^2}\exp\left\{-\frac{\tau_c}{t} - \frac{t}{\tau_L}\right\}, \quad (11)$$

where τ_c and τ_L are the rise and decay timescales, respectively, and E_k (p_k) is the particle's kinetic energy (momentum) at 0.05 au. In this work, γ_0 is the index of the source spectrum and is set to be 2.0. C is the normalization constant. In the calculation, τ_c and τ_L are set to be 0.0833 days and 0.1666 days, respectively. Since we consider the event-integrated spectrum in this work, the choice of τ_c and τ_L has no impact on our analysis. The time-integrated fluence F_{E_i} for energy E_i at 1 au is calculated by summing over the source file of all the particles that arrived at 0.05 au with final energy E_k,

$$F_{E_i} = \sum_k \int_0^T \int_{-1}^1 \frac{C}{t}\frac{E_k^{-\gamma_0}}{p_k^2}\exp\left\{-\frac{\tau_c}{t} - \frac{t}{\tau_L}\right\} d\mu dt. \quad (12)$$

In this work, different elements He, O, Mg, and Fe are considered; their charge states are summarized in Table 1 (e.g., Klecker et al. 2000; Mobius et al. 2000; Cohen et al. 2005). The charge states are rounded up in this work.

3. TURBULENCE SPECTRA

A particle's pitch-angle diffusion is determined by the interplanetary magnetic turbulence. The first observational evidence of the solar wind turbulence was made by *Mariner 2* magnetic and plasma observations. Observations showed that the solar wind is often turbulent with energy distributed over a wide frequency range (energy-containing range, inertial range, and dissipation range). A complete review of the solar wind turbulence can be found in Bruno & Carbone (2005).

In this work, we consider two forms of turbulence spectrum. One is a power law with index Γ

$$P(k) = A_0\frac{1}{k^\Gamma}, \quad (13)$$

and the other is

$$P(k) = A_1\frac{1}{1 + (kz_c)^\Gamma}. \quad (14)$$

Here A_0 and A_1 are the normalization constants, z_c is the correlation length, k is the wavenumber, and Γ is the spectral index. The turbulence expressed in Equation (13) only has the inertial range, while in Equation (14) both the energy-containing range and the inertial range are included. These two ranges adjoin at the break frequency (correlation length z_c).

The radial evolution of the power spectra of the interplanetary turbulence was first studied by Bavassano et al. (1982) and Denskat & NeuBauer (1983), using *Helios 2* s/c observations. It was later reproposed by Bruno & Carbone (2005) in their Figure 23. Power density spectra at different heliocentric distances of 0.3, 0.7, and 0.9 au were analyzed. They concluded that the break frequency moves to lower and lower ends as the solar wind expands. The same conclusion was made for 1, 2.8, and 5 au (Matthaeus & Goldstein 1982). In proportion to 1 au, SEPs experience all turbulence in the inner heliosphere. The effective spectral break of the turbulence experienced by SEPs is not known. In our treatment, it is a free parameter. The typical correlation length at 1 au is 1×10^9 m. For turbulence closer to the Sun, small correlation lengths are chosen: 5×10^8 m and 1×10^8 m.

In the calculation, turbulence strength is set to be such that the radial mean free path of 1 MeV proton is 0.005 au at all radial distances. A particle with rigidity R resonates with the wave with a wavenumber $k_r = B/(R|\mu|)$. At 1 au, for instance, the resonant wavenumber for a 1 MeV proton with pitch-angle cosine $\mu = 1$ is 3.6×10^{-8} m^{-1}. At the same energy per nucleon, particles with a different Q/A ratio resonate with a different k_r. For the power-law turbulence spectrum shown in Equation (13), particles having the same speed but different Q/A experience different turbulence levels. For the turbulence spectrum shown in Equation (14), not only do particles with a different Q/A experience different turbulence levels, but particles that resonate around the break frequency see the frequency break at a different energy per nucleon.

4. RESULTS

We performed two sets of simulations based on Equations (13) and (14). In the first set of simulations, the interplanetary turbulence is assumed to be power laws with index $\Gamma = 1.1$, 1.6, and 2.0. In the second set of simulations, the interplanetary turbulence is assumed to be in the form of Equation (14), with an index $\Gamma = 1.6$ and correlation lengths $z_c = 1 \times 10^9$ m, 5×10^8 m, and 1×10^8 m. The spectra of $P(k)$s are plotted in Figure 1. The black, red, and blue lines represent the first set of simulations, and the orange, green, and blue lines represent the second set of simulations.

In the first set of simulations, by substituting Equation (13) into Equation (10), a particle's mean free path can be written as

$$\lambda_\parallel \sim R^{2-\Gamma}. \quad (15)$$

As Γ increases from 1.1 to 2.0, the dependence of $\lambda_\parallel$ on R decreases from $R^{0.9}$ to R^0. The input radial mean free paths for He, Mg, O, and Fe, the resulting energy spectra, and the fitting spectra are shown in Figure 2. In the left column of Figure 2, panels (1a), (1b), and (1c) represent the case in which Γ equals 2.0; in the middle column, panels (2a), (2b), and (2c) represent the case in which Γ equals 1.6; in the right column, panels (3a), (3b), and (3c) represent the case in which Γ equals 1.1. The top row, panels (1a), (2a), and (3a), shows the input mean free paths in the three cases; the middle row, panels (1b), (2b), and (3b), shows the resulting energy spectra; and the bottom row,

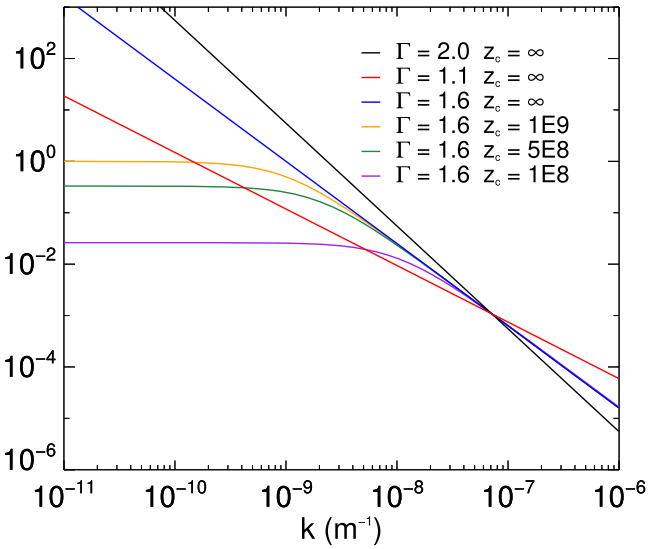

Figure 1. Sketch of the interplanetary power spectra used in the simulation. The black, blue, and red lines show the $P(k)$ when it obeys a power law with index of 2.0, 1.6, and 1.1. The orange, green, and purple lines show the $P(k)$ when it has the form of Equation (14), with a power index of 1.6 and correlation lengths of 1×10^9 m, 5×10^8 m, and 1×10^8 m. Those lines intersect at one point. This point represents the wavenumber k, at which a 1 MeV proton with pitch-angle cosine $\mu = 1$ resonates.

panels (1c), (2c), and (3c), shows the fitting result of the energy spectra using the form of Band et al. (1993). The fitting results are shifted downward for a better view. The fitting results are summarized in Table 2.

In case 1, when the turbulence power index is 2.0, the input mean free paths, shown in panel (1a), are the same at different energies for all the elements, consistent with the R^0 dependence. In panel (1b), the spectra of He, O, Mg, and Fe are plotted in black plus signs, red asterisks, blue diamonds, and orange triangles, respectively. Apparently, the spectra roll over at high energies. Furthermore, the rollover energy decreases as the element gets heavier. We then fit the energy spectra with the spectral form of Band et al. (1993). The fitting results are shown in panel (1c) and Table 2. The energy spectra are well fit with the double power laws (Equation (2)). The rollover energy per nucleon E_0 is 0.12 GeV nucleon^{-1} for He, with $Q/A = 0.5$; 0.095 GeV nucleon^{-1} for O, with $Q/A = 0.4375$; 0.08 GeV nucleon^{-1} for Mg, with $Q/A = 0.375$; and 0.065 GeV nucleon^{-1} for Fe, with $Q/A = 0.231$. The decreasing pattern is clearly seen.

In case 2, however, the input mean free path increases with energy because of the spectral index $\Gamma = 1.6$, leading to an $R^{0.4}$ dependence. At the same energy per nucleon, the mean free paths for different elements differ. The resulting spectra are shown in panel (2b), with the same legends as panel (1b). The spectra of low energies are flatter than those in case 1. Panel (2c) shows the fitting spectra with double power laws. The fitted parameters are shown in Table 2. The low-energy spectra have an index of 1.18, smaller than that in case 1, which has an index of 1.35. The rollover energy per nucleon is 0.09 GeV nucleon^{-1} for He, 0.08 GeV nucleon^{-1} for O, 0.06 GeV nucleon^{-1} for Mg, and 0.04 GeV nucleon^{-1} for Fe. In this case, the spectra of all elements bend over at lower energies than in case 1.

In case 3, the input mean free path has an even stronger dependence on a particle's rigidity $\lambda_\parallel \sim R^{0.9}$, and the difference between elements is also larger, as shown in panel (3a). Panel (3b) plots the resulting energy spectra for different elements, sharing the same legends as panel (1b). Compared to panel (1b) and panel (2b), the extent to which the energy spectra bend over is even larger, and the rollover energies are smaller. The fitting results are plotted in panel (3c), and the fitted parameters are summarized in Table 2. The rollover energy is 0.028 GeV nucleon^{-1} for He, 0.023 GeV nucleon^{-1} for O, 0.018 GeV nucleon^{-1} for Mg, and 0.01 GeV nucleon^{-1} for Fe.

From the first set of simulations, we conclude that a double power law at 1 au can be obtained by assuming a power law at the Sun through a pure transport process. In the same turbulence level $(\delta B)^2$, the harder the interplanetary turbulence power spectrum, the harder the low-energy spectrum at 1 au and the smaller the rollover energy. The break energy E_0 is ordered by the Q/A ratio: E_0(He) $>$ E_0(O) $>$ E_0 (Mg) $>$ E_0(Fe).

In the second set of simulations, the turbulence spectrum in the form of Equation (14) is assumed. By substituting Equation (14) into Equation (10), the input mean free path is then

$$\lambda_\parallel \sim R^{2-\Gamma} \int_0^1 (1-\mu^2)|\mu|^{1-\Gamma}((R\,|\mu|)^\Gamma + z_c^\Gamma)d\mu. \quad (16)$$

The index of the inertial range, Γ, is set to be 1.6. The correlation length, in different test cases, is set to 1×10^9 m, 5×10^8 m, and 1×10^8 m. The corresponding turbulence spectra are shown in Figure 1. Similar to Figure 2, in Figure 3 the first, second, and third columns show the simulation results for cases 4, 5, and 6, respectively. The first, second, and third rows show the input mean free paths, the resulting spectra, and the fitting spectra, respectively.

In case 4, the correlation length is set to be 1×10^9 m, which is the typical value at 1 au. In panel (4a), compared with panel (2a), which has a correlation length of infinity, the mean free path of high-energy particles is larger. The fitting spectra are shown in panel (4c). Again, a good fit with double power laws is obtained. The fitted parameters are summarized in Table 3. The fitted low- and high-energy spectra indices are a little bit larger than those obtained in case 2. The rollover energy is 0.06 GeV nucleon^{-1} for He, 0.055 GeV nucleon^{-1} for O, 0.048 GeV nucleon^{-1} for Mg, and 0.032 GeV nucleon^{-1} for Fe. The heavier the element, the lower the rollover energy. Generally speaking, the rollover energies in case 4 are smaller than those in case 2. Therefore, we conclude that including the energy-containing range in the turbulence spectrum helps those high-energy particles diffuse away quickly from 1 au. Furthermore, the heavier the elements (smaller Q/A ratio), the smaller the energies per nucleon at which particles start to resonate in the energy-containing range.

In case 5, we assume the correlation length to be 5×10^8 m. From panel (5a), the particles' mean free paths increase much more rapidly than those in case 4. In panel (5b), the energy spectra bend over at even lower energies than in panel (4b). The fitting spectra are plotted in panel (5c), and the fitted parameters are summarized in Table 3. The spectral index for low energies does not vary much from case 4; however, the high-energy spectral indices are larger than in case 4. The break energy is 0.043 GeV nucleon^{-1} for He, 0.04 GeV nucleon^{-1} for O, 0.036 GeV nucleon^{-1} for Mg, and 0.03 GeV nucleon^{-1} for Fe. Overall, spectra break at lower energies than in case 4.

In case 6, the turbulence correlation length is set to be 1×10^8 m, even smaller than in case 5. The input mean free

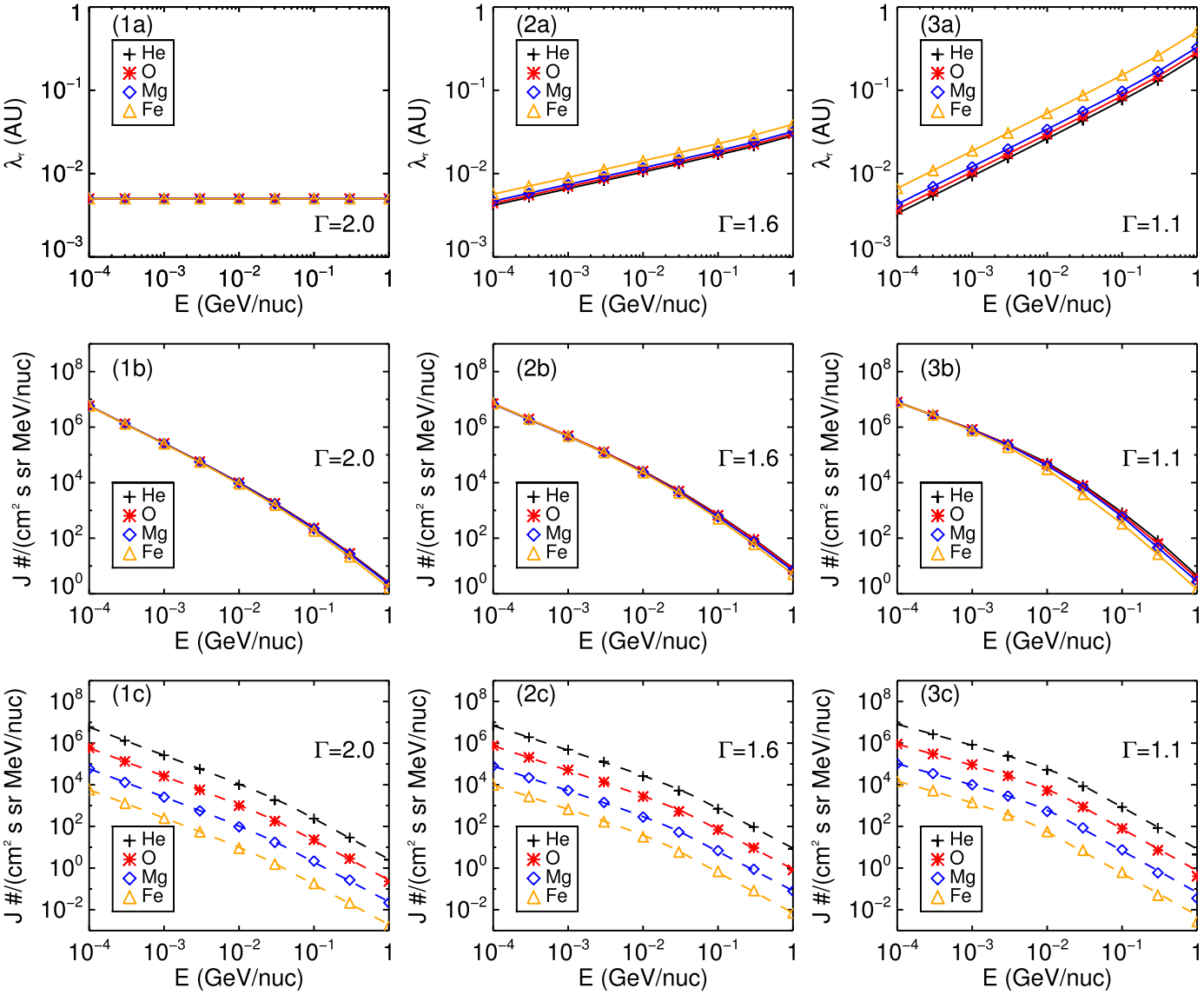

Figure 2. Results for the first set of simulations: cases 1, 2, and 3. Each case is shown in one column. The left column represents the case in which the power spectrum index is 2.0, the middle column represents the case in which the index is 1.6, and the right column represents the case in which the index is 1.1. The top row shows the input radial mean free path for different elements at different energies, with He in black plus signs, O in red asterisks, Mg in blue diamonds, and Fe in orange triangles. The middle row shows the resulting spectra at 1 au. The bottom row shows the fitting spectra using the form of Band et al. (1993).

paths, plotted in panel (6a), increase even more rapidly than in panel (5a). The mean free paths of elements He, O, and Mg are greater than 1 au at 1 GeV nucleon^{-1}. The mean free path of element Fe is greater than 1 au at energies larger than 0.3 GeV nucleon^{-1}. In this work, $\int_{-1}^{1} f d\mu$ is calculated by $f(\mu = 1) + f(\mu = -1) + 2f(\mu = 0)$ based on the second-order harmonic expansion. When the mean free path is greater than 1 au, $f(\mu = 0)$ and $f(\mu = -1)$ approach zero. Then $f(\mu = 1) + f(\mu = -1) + 2f(\mu = 0)$ is not a good approximation of $\int_{-1}^{1} f d\mu$ anymore. Therefore, we only calculate and plot the energy spectra up to 0.3 GeV nucleon^{-1} for He, O, and Mg, and up to 0.1 GeV nucleon^{-1} for Fe in panels (6b) and (6c). The fitting spectra are plotted in panel (6c), and the fitted parameters are summarized in Table 3. The energy spectra break at even smaller energies, with $E_0 = 0.03$ GeV nucleon^{-1} for He, 0.028 GeV nucleon^{-1} for O, 0.025 GeV nucleon^{-1} for Mg, and 0.013 GeV nucleon^{-1} for Fe.

In the second set of simulations, we investigate the effect of different correlation lengths on the energy spectral break. We conclude that the smaller the correlation length, the lower energies at which the energy spectra tend to break. Also the break energies decrease as the elements get heavier.

To better compare different cases, we plot the mean free paths and the fitted energy spectra for oxygen in these six cases in Figures 4 and 5. Similar to Figure 1, the black, red, and blue curves represent the cases, assuming that the interplanetary turbulence is a power spectrum with indices 2.0, 1.1, and 1.6. The orange, green, and purple lines represent the cases, assuming that the interplanetary turbulence has a correlation length of 1×10^9 m, 5×10^8 m, and 1×10^8 m. The spectra in Figure 5 are shifted downward for a better view.

The break energies E_0 versus Q/A in those six cases are plotted in Figure 6. The legend is the same as in Figure 1. If the turbulence spectra are pure power law, the break energies E_0 decrease as the power-law index Γ decreases. If the turbulence

Table 2
Fitting Parameters for Cases 1, 2, and 3

Case	He			O			Mg			Fe		
	α	β	E_0 (GeV nuc^{-1})	α	β	E_0 (GeV nuc^{-1})	α	β	E_0 (GeV nuc^{-1})	α	β	E_0 (GeV nuc^{-1})
1	1.35	1.95	0.120	1.35	1.90	0.095	1.35	1.90	0.080	1.35	1.93	0.065
2	1.18	1.90	0.090	1.18	1.90	0.080	1.18	1.88	0.060	1.15	1.95	0.040
3	1.00	2.00	0.028	1.00	2.00	0.023	1.00	2.00	0.018	2.00	2.00	0.010

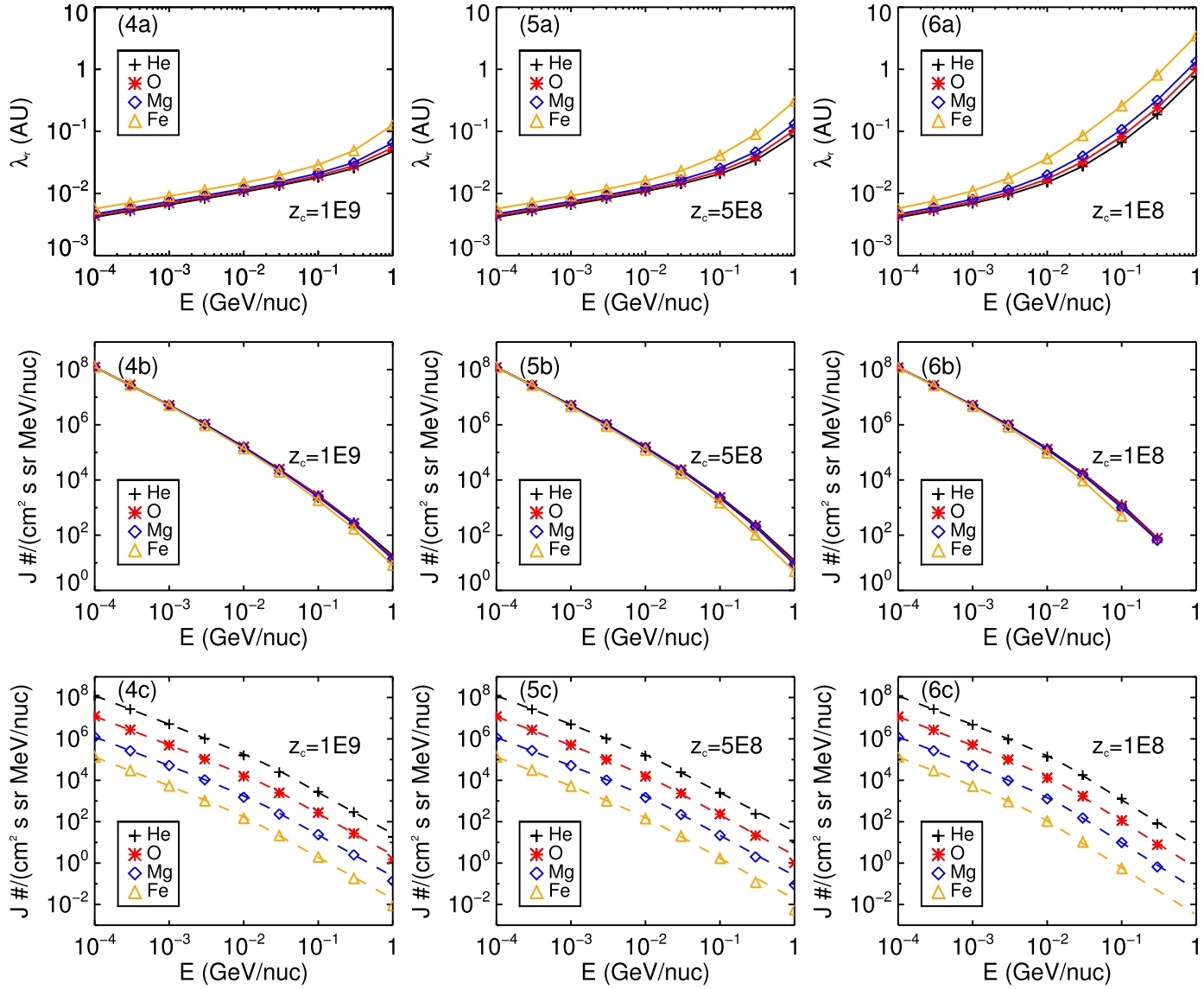

Figure 3. Results for the second set of simulations: cases 4, 5, and 6. Similar to Figure 2, each case is shown in one column. All of the cases have a power spectrum index of 1.6 for the inertial range. The left column represents the case in which the correlation length is 1×10^9 m; the middle column represents the case in which the correlation length is 5×10^8 m; and the right column represents the case in which the correlation length is 1×10^8 m. The top row shows the input radial mean free path for different elements at different energies. He is plotted in black plus signs, O in red asterisks, Mg in blue diamonds, and Fe in orange triangles. The middle row shows the resulting spectra at 1 au. The bottom row shows the fitting spectra using the form of Band et al. (1993).

spectra obey a power law with a correlation length z_c, the break energy decreases as z_c decreases. The break energy E_0 also correlates with Q/A by $E_0 \sim (Q/A)^{\delta}$. The value of δ ranges from 0.4 to 1.3 from the fitting. The fitted low-energy spectral index α versus Q/A and the fitted high-energy spectral index β versus Q/A are plotted in Figure 7 (panels (a) and (b), respectively).

5. DISCUSSION

The spectral break can be obtained by solving the focused transport equation (Equation (3)) under certain approximations. If the distribution function f is assumed to be nearly isotropic, then it can be expanded in a series of Legendre polynomials $P_i(\mu)$, $f = 1/2(f_0 + f_1\mu)$. Here f_0 is the isotropic part, f_1 is the first-order anisotropy part, and we neglect the higher-order

Table 3
Fitting Parameters for Cases 4, 5, and 6

Case	He			O			Mg			Fe		
	α	β	E_0 (GeV nuc^{-1})	α	β	E_0 (GeV nuc^{-1})	α	β	E_0 (GeV nuc^{-1})	α	β	E_0 (GeV nuc^{-1})
4	1.38	2.00	0.060	1.38	2.00	0.055	1.38	2.00	0.048	1.38	2.00	0.032
5	1.38	1.87	0.043	1.38	1.95	0.040	1.36	1.95	0.036	1.40	1.98	0.030
6	1.38	2.25	0.030	1.38	2.25	0.028	1.38	2.27	0.025	1.38	2.27	0.013

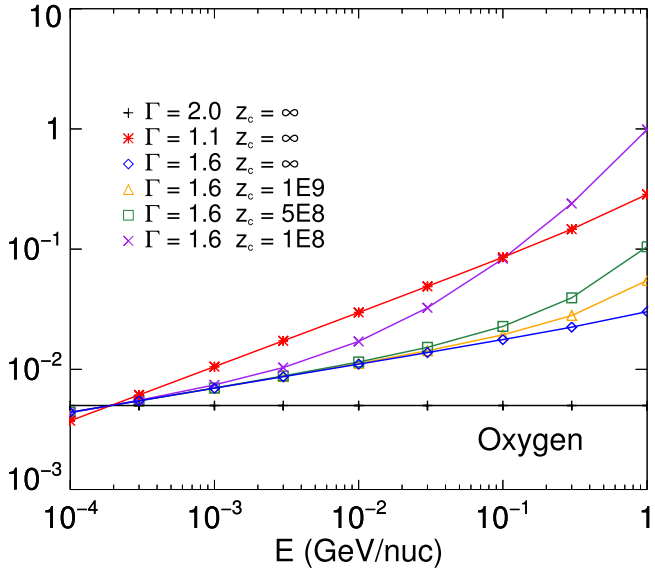

Figure 4. Input radial mean free paths for oxygen in the six cases. The black, blue, and red lines represent the cases in which the interplanetary turbulence obeys a power spectrum with the indices of 2.0, 1.6, and 1.1, respectively. The orange, green, and purple lines show the cases in which the interplanetary turbulence spectrum is in the form of Equation (14), with an index of 1.6 and correlation lengths of 1×10^9 m, 5×10^8 m, and 1×10^8 m, respectively.

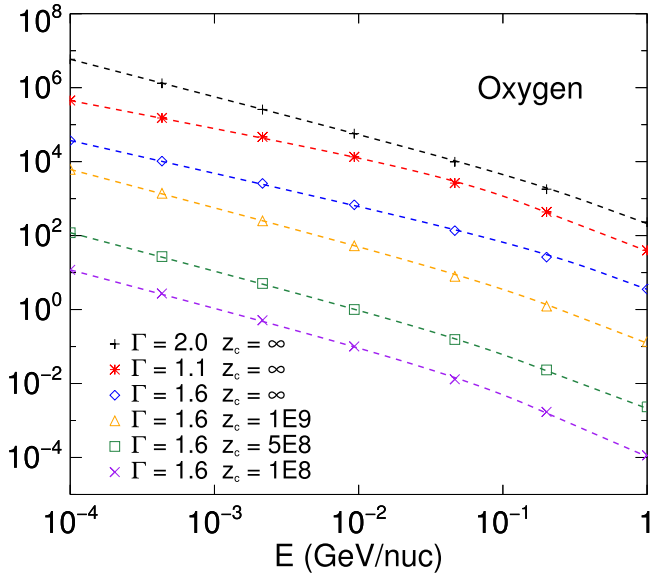

Figure 5. Resulting and fitting spectra for oxygen in the six cases. Cases 1, 2, and 3 are represented by the black plus signs, blue diamonds, and red asterisks, respectively. Cases 4, 5, and 6 are represented by the orange triangles, green squares, and purple crosses, respectively. Spectra are shifted downward with respect to each other for a better view.

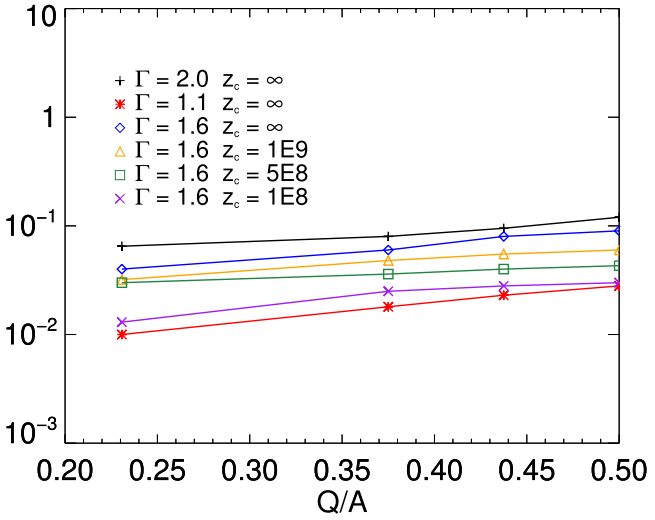

Figure 6. Break energy E_0 vs. the particle's charge-to-mass ratio (Q/A) in six cases.

terms. Substituting f into Equation (3) and integrating over μ, we get (e.g., Parker 1965; Jokipii 1968)

$$\frac{\partial f_0}{\partial t} = \frac{1}{r^2}\frac{\partial}{\partial r}\left(\frac{1}{r^2}D_{rr}\frac{\partial f_0}{\partial r}\right) - V^{\rm sw}\nabla f_0 + \frac{2V^{\rm sw}}{3r}p\frac{\partial f_0}{\partial p} + \int_{-1}^{1} Q d\mu. \quad (17)$$

D_{rr} is the radial diffusion coefficient, and it relates to the particle's radial mean free path λ_r by $D_{rr} = 1/3v\lambda_r$. By integrating Equation (17) over t from 0 to T, the event-integrated fluence $F = \int_0^T f_0 dt$ then satisfies

$$\frac{1}{r^2}\frac{\partial}{\partial r}\left(\frac{1}{r^2}D_{rr}\frac{\partial F}{\partial r}\right) - V^{\rm sw}\frac{\partial F}{\partial r} + \frac{2V^{\rm sw}}{3r}p\frac{\partial F}{\partial p} + C_0 p^{-2\gamma_0-2} = 0, \quad (18)$$

where C_0 is a constant from the contribution of the source. In order to solve Equation (18) analytically, we approximate the first term and the second term by F/τ_1 and F/τ_2, respectively. If τ_1 and τ_2 are further assumed to be independent of a particle's momentum for simplicity, we solve F as

$$F = -\frac{C_0}{\kappa - 2\gamma - 2}p^{-2\gamma-2} + C_1 p^{-\kappa}, \quad (19)$$

where

$$\kappa = \frac{3r}{2V^{\rm sw}}\left(\frac{1}{\tau_1} - \frac{1}{\tau_2}\right),$$

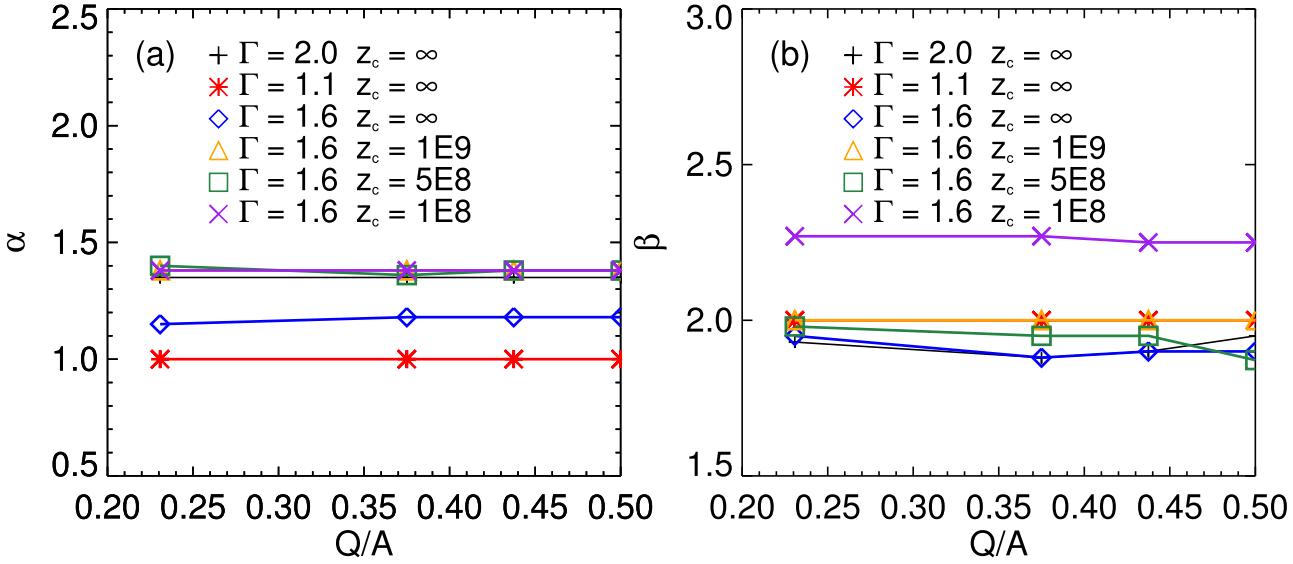

Figure 7. (a) Fitted low-energy spectral index α and (b) high-energy spectral index β vs. the particle's charge-to-mass ratio (Q/A) in six cases.

and C_1 is a constant from the integration. A double power law with index $-\gamma$ and $-(\kappa - 2)/2$ is obtained for a particle's differential fluence.

Shown in Table 4, we calculate the first three terms in Equation (18) at 1 au. In the calculation, we assume that the interplanetary turbulence spectrum is a power law with an index of 1.6. Four energies per nucleon (100 keV nucleon^{-1}, 300 keV nucleon^{-1}, 30 MeV nucleon^{-1}, and 100 MeV nucleon^{-1}) of O are considered. The spectral index, $(\kappa - 2)/2$, is also calculated at different energies, shown in the last column. At lower energies, $(\kappa - 2)/2$ is small, yielding harder spectra than the source profile. At higher energies, $(\kappa - 2)/2$ is large, which results in softer spectra. The trend of the spectral indices is consistent with the results shown in Figure 7.

The analytical solution of Equation (18) with a monoenergetic injection profile was given by Webb & Gleeson (1974). A constant radial solar wind and a diffusion coefficient $D_{rr} \sim D_0(p)r^{\eta}$ were assumed. Here $D_0(p)$ is a function of the particle's momentum. In Li & Lee (2015), the solution of Equation (18) with a power-law injection profile was found by performing the convolution of the solution in Webb & Gleeson (1974) with the power-law injection profile. In their calculation, several simplifications and approximations were made. Three distinctive power laws were obtained at 1 au with break energies satisfying $V^{sw}r/D_{rr} \sim 1$ or $V^{sw}r/D_{rr} \sim (r/r_s)^{(2/3)\chi}$. Here $\chi = 2\Gamma$ and r_s is the location of the shock. $D_0(p)$ was assumed to be proportional to $p^{3-\Gamma}$. $V^{sw}r/D_{rr} \sim (r/r_s)^{(2/3)\chi}$ predicts the energy break at a low-energy range, which is less than tens of keV per nucleon, below the lowest energy we considered in our simulation. $V^{sw}r/D_{rr} \sim 1$ predicts the energy break at a high-energy range. In case 1, Γ is assumed to be 2.0. Then $V^{sw}r/D_{rr} \sim 1$ predicts a break energy of 288 MeV nucleon^{-1} for He, which is larger than 120 MeV nucleon^{-1} from our fitting. If we assume $\Gamma = 1.6$, which is case 2, $V^{sw}r/D_{rr} \sim 1$ predicts a break energy of $E_0 \sim 38$ MeV nucleon^{-1} for He, which is smaller than 90 MeV nucleon^{-1} shown in Table 2, but close to the value of 43 MeV nucleon^{-1} in case 5. In case 3, Γ is assumed to be 1.1 and $V^{sw}r/D_{rr} \sim 1$ predicts a break energy of 10 MeV nucleon^{-1} for He, smaller than 28 MeV nucleon^{-1} from our fitting. The differential spectral index predicted by Li & Lee (2015) is $\alpha = \gamma_0 - (3 - \Gamma)(2\gamma_0 - 1)/(4\Gamma)$ for the low-energy end and $\beta = \gamma_0 - (\Gamma - 3)/2$ for the high-energy end. Substituting the parameters used in case 2, we get $\alpha = 1.34$ and $\beta = 2.70$. The differential spectra predicted by the analytical model (Li & Lee 2015) are overall softer than that in the numerical simulation, $\alpha = 1.18$ and $\beta = 1.90$. However, their results are more consistent with those in case 6, in which the correlation length is 1×10^8 m.

Table 4
Numerical Calculation for the Terms in Equation (18)

Energy per Nucleon (GeV nuc^{-1})	Diffusion	Adiabatic Cooling	Convection	$(\kappa - 2)/2$
1E-4	1.1	−3.4E1	−1.3E2	0.94
3E-4	3.4E-1	−2.8E-1	−9.1	0.90
3E-2	4.2E-4	−7.3E-5	−1.7E-4	3.73
1E-1	3.7E-5	−1.3E-4	−7.1E-6	7.93

In our simulation, D_{rr} is assumed to be radially independent, while in Li & Lee (2015), D_{rr} was assumed to be proportional to $r^{3-2\Gamma}$. This may be one possible cause of the difference. Another possible cause of the difference between our simulation and that of Li & Lee (2015) may arise from the criteria that Li & Lee (2015) used to simplify the solution. In Li & Lee (2015), the $V^{sw}r/D_{rr} \sim 1$ criterion comes from the assumption that the adiabatic cooling effect of high-energy -particles is negligible, i.e., $p/p_0 \sim 1$, where p_0 is the particle's initial momentum. Nevertheless, from our simulation, in case 2, we found that, for 100 MeV nucleon^{-1} He, there are still 44% of particles that lose more than 50% of their initial momentum. In case 5, the percentage drops to 38%. Only in case 6 do 1.3% of particles lose more than 50% of their initial momentum, which is consistent with the assumption made by Li & Lee (2015). In other cases, although the conditions do not match Li & Lee (2015), we still get a double power-law spectrum. This demonstrates that the double power-law spectrum is a robust effect of interplanetary propagation.

We deduced the break velocity from $V^{\rm sw}r/D_{rr} \sim 1$ as

$$v_0 \sim r^{1/(3-\Gamma)}\left(\frac{3V^{\rm sw}}{\lambda_{\rm 1\,MeV}}\right)^{1/(3-\Gamma)}(v_{\rm 1\,MeV})^{(2-\Gamma)/(3-\Gamma)} \times (Q/A)^{(2-\Gamma)/(3-\Gamma)}, \quad (20)$$

where $\lambda_{\rm 1\,MeV}$ is the radial mean free path of 1 MeV proton at 1 au and $v_{\rm 1\,MeV}$ is the speed of a 1 MeV proton. Here we assume that D_{rr} is independent of r and get $v_0 \sim r^{1/(3-\Gamma)}$. If we assume that D_{rr} is proportional to $r^{3-2\Gamma}$, we get $v_0 \sim r^{(2\Gamma-2)/(3-\Gamma)}$. The break velocity v_0 increases as r increases, if $1 < \Gamma < 3$. However, in our simulation, we find that v_0 decreases as r increases. For example, in case 6, the break energy for Fe is 44 MeV nucleon^{-1} at 0.2 au, 16 MeV nucleon^{-1} at 0.5 au, and 13 MeV nucleon^{-1} at 1 au. In Equation (20), the break energy of different elements scales by the charge-to-mass ratio $(Q/A)^{\delta}$, with $\delta = 2(2-\Gamma)/(3-\Gamma)$. δ only depends on the interplanetary turbulence spectrum index. In our simulation, δ also varies with different correlation length z_c. All these suggest that the criterion for spectral break is more complicated than $V^{\rm sw}r/D_{rr} \sim 1$ of Li & Lee (2015) derived from the assumption of $p/p_0 \sim 1$.

6. CONCLUSION

In this paper, we investigate the effect the interplanetary transport on the event-integrated energy spectra observed at 1 au through a focused transport approach. A time-backward Markov stochastic process is used to trace energetic particles from 1 au back to the Sun, where the energy spectrum is assumed to be a pure power law. Different forms of turbulence spectra are examined. In this work, we found that the interplanetary transport can lead to a double power-law spectrum at 1 au, with the break energies correlating with a particle's Q/A ratio, a conclusion similar to Li & Lee (2015). However, we found that the formation of the double power-law spectrum is far more robust than in the condition assumed by Li & Lee (2015). The break energies of different elements correlate with particles' charge-to-mass ratio (Q/A) by $E_0 \sim (Q/A)^{\delta}$. The index δ varies from 0.4 to 1.3 with different prescribed interplanetary turbulence. A break energy ranging from 10 to 120 MeV nucleon^{-1} is obtained in different cases. By assuming a pure power turbulence spectrum, the smaller the turbulence index Γ, the smaller the break energy. We also found that including the energy-containing range helps the particles' spectra to break at lower energies. The smaller the correlation length, the smaller the break energy.

The authors would like to acknowledge the discussion with Gen Li and Martin Lee. The authors also thank Gang Li for his suggestions. This work was supported in part by NSF Grant AGS-1156056, NASA Grants NNX14AJ53G, NNX15AN72G, and NNX15AB76G, and DOE Grant DE-SC0008721.

REFERENCES

Axford, W. I., Leer, E., & Skadron, G. 1977, ICRC, 11, 132
Band, D., Matteson, J., Ford, L., et al. 1993, ApJ, 413, 281
Bavassano, B., Dobrowolny, M., Mariani, F., & Ness, N. F. 1982, JGR, 87, 3617
Blandford, R. D., & Ostriker, J. P. 1978, ApJL, 221, L29
Bruno, R., & Carbone, V. 2005, LRSP, 2, 4
Cohen, C., Mewaldt, R. A., Cumming, C. A., et al. 2003, AdSpR, 32, 101
Cohen, C. M. S., Stone, E., Mewaldt, R. A., et al. 2005, JGR, 110, A09S16
Decker, R. B. 1988, SSRv, 48, 195
Denskat, K. U., & NeuBauer, F. M. 1983, in Proc. Conf. 2280, Solar Wind Five, ed. M. Neugebauer, 81
Earl, J. A. 1974, ApJ, 193, 231
Ellison, D. C., & Ramaty, R. 1985, ApJ, 298, 400
Isenberg, P. A. 1997, JGR, 102, 4719
Jokipii, J. R. 1966, ApJ, 146, 480
Jokipii, J. R. 1968, JGRA, 73, 5495
Jokipii, J. R. 1971, RvGSP, 9, 27
Klecker, B., Bogdanov, A. T., Popecki, M., et al. 2000, in AIP Conf. Proc. 528, Acceleration and Transport of Energetic Particles Observed in the Heliosphere (Melville, NY: AIP), 135
Kóta, J., & Jokipii, J. 1997, ICRC, 1, 213
Krymsky, G. F. 1977, DoSSR, 234, 1306
Lee, M. A. 1983, JGR, 88, 6109
Lee, M. A., & Lerche, I. 1974, RvGSP, 12, 671
Li, G., & Lee, M. A. 2015, ApJ, 810, 82
Li, G., & Zank, G. P. 2005, GeoRL, 32, L02101
Li, G., Zank, G. P., Verkhoglyadova, O., et al. 2009, ApJ, 702, 998
Mason, G. M., Li, G., Cohen, C. M. S., et al. 2012, ApJ, 761, 104
Matthaeus, W. H., & Goldstein, M. L. 1982, JGR, 87, 6011
Mazur, J. E., Mason, G. M., Klecker, B., & McGuire, R. E. 1992, ApJ, 401, 398
Mewaldt, R. A., Cohen, C. M. S., Labrador, A. W., et al. 2005a, JGRA, 110, 1
Mewaldt, R. A., Looper, M. D., Cohen, C., et al. 2005b, ICRC, 101, 111
Mewaldt, R. A., Looper, M. D., Cohen, C. M. S., et al. 2012, SSRv, 171, 97
Miller, J. A. 1998, SSRv, 86, 79
Mobius, E., Klecker, B., Popecki, M. A., et al. 2000, in AIP Conf. Proc. 528, Acceleration and Transport of Energetic Particles Observed in the Heliosphere (Melville, NY: AIP), 131
Parker, E. N. 1965, P&SS, 13, 9
Qin, G., Zhang, M., & Dwyer, J. R. 2006, JGR, 111, A08101
Qin, G., Zhang, M., Dwyer, J. R., & Rassoul, H. K. 2004, ApJ, 609, 1076
Reames, D. V. 2013, SSRv, 175, 53
Reid, G. C. 1964, JGR, 69, 2659
Roelof, E. C. 1969, in Lectures in High-Energy Astrophysics, ed. H. Ögelman & J. R. Wayland (Washington, DC: NASA), 111
Skilling, J. 1971, ApJ, 170, 265
Tylka, A. J., Boberg, P. R., Cohen, C. M. S., et al. 2002, ApJ, 581, 119
Tylka, A. J., Boberg, P. R., Mcguire, R. E., Ng, C. K., & Reames, D. V. 2000, in AIP Conf. Proc. 528, Acceleration and Transport of Energetic Particles Observed in the Heliosphere (Melville, NY: AIP), 147
Tylka, A. J., Cohen, C. M. S., Dietrich, W. F., et al. 2005, ApJ, 625, 474
Tylka, A. J., Dietrich, W. F., & Boberg, P. R. 1997, ICRC, 1, 101
Tylka, A. J., & Lee, M. A. 2006, ApJ, 646, 1319
Webb, G. M., & Gleeson, L. J. 1974, PASAu, 2, 299
Wentzel, D. G. 1974, ARA&A, 12, 71
Zank, G. P., Rice, W. K. M., & Wu, C. C. 2000, JGR, 105, 25079
Zhang, M. 1999, ApJ, 513, 409
Zhang, M. 2006, JGR, 111, A04208
Zhang, M., Qin, G., & Rassoul, H. 2009, ApJ, 692, 109